Dynamics and Control of Granular Imaging Systems[1]

Marco B. Quadrelli[2], Scott Basinger[3], David Palacios[4], Darmindra Arumugam[5]
Jet Propulsion Laboratory, California Institute of Technology, 4800 Oak Grove Drive, Pasadena, CA 91109-8099,

In this paper, we present some ideas regarding the modeling, dynamics and control aspects of *granular spacecraft*. Granular spacecraft are complex multibody systems composed of a spatially disordered distribution of a large number of elements, for instance a cloud of grains in orbit. An example of application is a spaceborne observatory for exoplanet imaging, where the primary aperture is a cloud instead of a monolithic aperture. A model is proposed of the multi-scale dynamics of the grains and cloud in orbit, as well as a control approach for cloud shape maintenance and alignment, and preliminary simulation studies are carried out for the representative imaging system.

I. Introduction

The useful engineering properties of a cloud of granular matter in space are virtually unknown. Granular matter is Tconsidered to be the 5th state of matter (after solid, liquid, gaseous, and plasma) by virtue of its peculiar response characteristics (cohesiveness, fluid behavior, compactification, phase transformation capability, and others) [6]. However, it is a fact that the dynamics, controllable properties, and consequent benefits of engineering and manipulating granular matter such as dust grains, powders, and granular spacecraft is poorly known to the space exploration community.

"Orbiting Rainbows" is a Phase II NASA Innovative Advanced Concepts (NIAC) study that is looking twenty years into the future of creating a space-based observatory from granular media. The goal of this research is to identify ways to optically manipulate and maintain the shape of a cloud of dust-like matter so that it can function as an adaptive surface with useful electromagnetic characteristics in the optical or microwave bands. The investigators are performing fundamental research and developing the technology roadmap to construct an optical system in space using nonlinear optical properties of a cloud of micron-sized particles, shaped into a specific surface by light pressure, to form a very large and lightweight aperture of an optical system. This "cloud optic" will be relatively simple to package, transport, and deploy. It is reconfigurable and can be re-targeted; the focal length is variable and it will be self-healing and ultimately disposable. With near-term plans to build 30 meter ground-based telescopes for astronomy, the demand for higher resolution optics in space continues to grow not only for exo-planet detection, but also for earth-based science, including hyper-spectral imaging and for monitoring of the oceans and land masses (e.g. seismic monitoring).

Three things make Orbiting Rainbows unique:

- The avoidance of any physical structure and sensing/actuation hardware on the primary, so sensing and actuation are done "at-a-distance" on an amorphous cloud, and all operational complexity is done outside the primary,
- The reliance on optical trapping and manipulation to enable that action "at-a-distance" (although, other mechanisms such as electrodynamic trapping and confinement are also being investigated), and
- The relaxation of the requirements on the fine cloud control by doing the best possible job in software via robust computational imaging algorithms.

[1] This research was carried out at the Jet Propulsion Laboratory, California Institute of Technology, under a contract with the National Aeronautic and Space Administration.
[2] Research Technologist and Group Lead, Mobility and Robotic Systems Section, Mail Stop 198-219, Associate AIAA Fellow
[3] Group Supervisor, Wavefront Sensing and Control, Mail Stop 306-451.
[4] Research Technologist, Wavefront Sensing and Control, Mail Stop 306-451.
[5] Research Technologist, Radar Concepts and Formulation Group, Mail Stop 198-219

As part of our investigation, we have considered refractive, reflective and holographic systems and outlined optical correction and collection systems. An optical imaging system design has been selected as the best candidate architecture for a space system involving a cloud. The sequence of optics is as follows: the starlight is focused by granular spacecraft optic "patch", creating a spherical wavefront. Light from all patches converges at an intermediate focus, which has an image-plane coded aperture. The light then reflects off secondary mirror (Gregorian) and the light from each patch is collimated. Each beam goes to a separate adaptive optics system. A fast steering mirror and a deformable mirror correct pointing and low to mid-spatial frequency aberrations. An optical delay line is used to correct phasing difference between the patches and allow for Fourier transform spectroscopy. A beam-splitter is included to allow some of the light to go to a Shack-Hartmann sensor to measure aberrations in the system. Imaging architectures in the radar band are also been considered, with the goal of focusing scattered energy to obtain higher resolution imaging or imaging in areas of the body that were previously inaccessible. We have developed a vector radiative transfer method for use with short wavelength radar instruments, and a Rayleigh or small particle approximation method for use with long wavelength radar instruments. This has been done with the intent to develop two radar instrument architectures to obtain higher-resolution remote sensing: a) a radar imaging architecture for topographic mapping; and b) a radar sounding architecture for subsurface or ionospheric sounding.

A study is also being conducted to determine the electromagnetic forces and torques experienced by a single grain under coherent illumination, in order to determine the conditions to achieve optical cooling. In this case, the assumptions used are that each grain is a rigid body, with nutation, precession, and spin as degrees of freedom, with the shape of a truncated cylinder with hemispherical cross-section. The grain material has its own index of refraction, the outside medium is vacuum, and the flat side of the grain is reflective. A commercial geometric ray-tracing code was used to obtain gradient/scattering force distribution. The light intensity is modulated by a proportional-integral-derivative (PID) feedback loop to reduce the error between the actual and desired nutation to zero, so that the light intensity modulation drives grain alignment in 3D. A representative cloud with varying number of grains is simulated to identify the limitations in computation time as the number of grains grows. We can derive a control law to track a desired surface in the Orbiting Reference Frame (ORF), equivalently to maintain a reference cloud shape, as follows. Finally, a laboratory model of a thin swarm of reflectors was built by randomly adhering small mirrors across the concave surface of a blackened parabolic reflector. In this experiment, the piston and pitch of the elements are randomized, but stationary. A collimated laser beam, collinear with the axis of the parabolic reflector was used to determine the point-spread function speckle pattern. The laser was then removed to allow the parabola to collect light from a scene of distant paraxial point sources. The measured speckles, combined with the PSF, were used reconstruct an image of the paraxial scene. Ideal image recovered from measured image by minimization process of an error metric. An iterative blind deconvolution technique was used to retrieve the image in the presence of noise (photon noise, dark current noise), and reconstruct the original image. These developments are described elsewhere.

In this paper, we present some ideas regarding the modeling, dynamics and control aspects of *granular spacecraft*. Granular spacecraft are complex multibody systems composed of a spatially disordered distribution of a large number of elements, for instance a cloud of N grains in orbit, with $N>10^3$. We address the modeling and autonomous operation of a distributed assembly (the cloud) of large numbers of highly miniaturized space-borne elements (the grains). A granular spacecraft can be defined as a collection of a large number of space-borne elements (in the 1000s) designed and controlled such that a desirable collective behavior emerges, either from the interactions among neighboring grains, and/or between the grains and the environment. The ultimate objective would be to study the behavior of the single grains and of large ensembles of grains in orbit and to identify ways to guide and control the shape of a cloud composed of these grains so that it can perform a useful function in space, for instance, as an element of an optical imaging system for astrophysical applications. This concept, in which the aperture does not need to be continuous and monolithic, would increase the aperture size several times compared to large NASA space-borne observatories currently envisioned such as ATLAST, allowing for a true Terrestrial Planet Imager that would be able to resolve exo-planet details and do meaningful spectroscopy on distant worlds. To accomplish this goal, we need to investigate the conditions to manipulate and maintain the shape of an orbiting cloud of dust-like matter so that it can function as an ultra-lightweight surface with useful and adaptable electromagnetic characteristics.

Consider the following scenario, shown in Figure 1: 1) the cloud is first released; 2) it is contained by laser pressure to avoid dissipation and disruption by gravitational tidal forces, 3) it is shaped by optical manipulation into

a two-dimensional object (coarse control), and 4) ultimately into a surface with imaging characteristics (fine control). The cloud shape has to be maintained against orbital disturbances by continuous figure control, also achieved optically. Applying differential light pressure retargets the entire cloud, so that a change of the optical axis can be induced. Selected parts of the cloud are reshaped when required for wavefront control, thus enabling higher quality optics. The entire imaging system is now in full operation, as 5) a multilens system searching for exo-planets, or 6) as a radio receiver engaged in remote sensing investigations. The potential advantages of the granular spacecraft concept are that: a) it can result in an ultra-lightweight system, made of very simple, very low cost, units; b) it can be very big: the cloud can distribute itself to kilometer scales, without the need to fill the aperture; c) the cloud is easy to package, transport and deploy; d) it is reconfigurable, and can be retargeted and repointed with non-mechanical means; e) the cloud is a highly fault-tolerant system with very low vulnerability to impacts. Other potential advantages offered by the cloud properties as optical system involve possible combination of properties (combined transmit/receive), variable focal length, combined refractive and reflective lens designs, and hyper-spectral imaging.

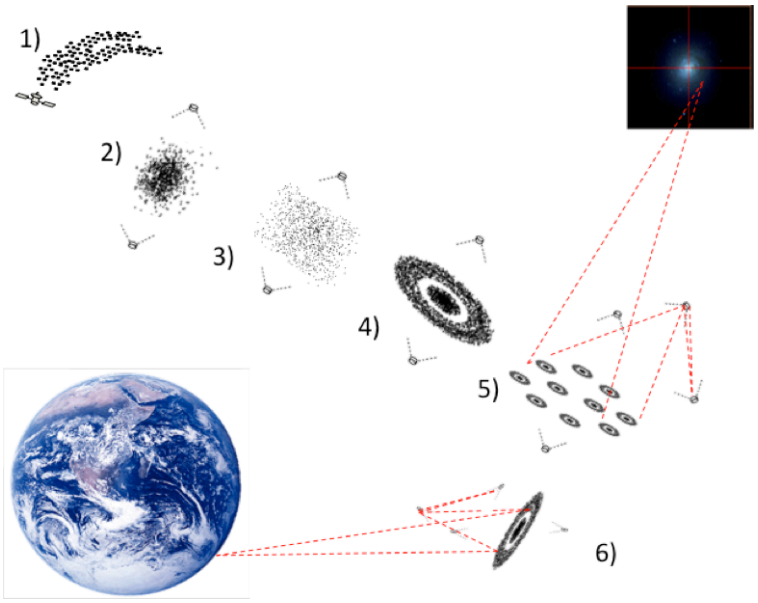

Figure 1. ***Scenario of application of a granular spacecraft.***

The study of granular spacecraft involves different disciplines: gravito-electrodynamics, optics, laser-matter interaction, disordered and distributed systems, multi-scale simulation, formation-flying, granular media, and plasma physics, among others. Because it is such a complex problem, this paper only scratches the surface and proposes a systemic view by first making some integrated modeling considerations in section 2, discussing the physics of the problem in Section 3, the control in Sections 4, 5, and 6, the electromagnetic scattering problem in the radar band in section 7, and a discussion of numerical simulation results in Section 7.

II. Integrated Modeling

Figure 2 describes the overall control architecture for our system model. It starts in the left with the particle simulation engine. This engine computes the motions of the particles that make up the primary optic at the granular level. It will be modified as necessary as data from the planned laboratory experiments becomes available. The micro-scale control system of the particles has the purpose to "corral" the particles, keep them functioning as unit, and ensure the optical properties of the conglomerate meet the requirements for the next stages of control. From the position and orientation of the particles, a complex electromagnetic pupil function is computed, from which the optical figure and pupil can be determined. The next stage of control is maintaining the relative position and

orientation of the separate spacecraft imaging system. The spacecraft has its own thrusters and reaction wheels to maintain precision optical alignment using a laser metrology truss developed at JPL as a precision sensor. Next is the mid-level control systems. A STOP (Structural, Optical) model of a single patch/cloud and its corresponding correction/collections system is needed for the Wavefront Sensing and Control (WFSC). Drivers to the STOP model include thermal variations based on the trajectory of the system relative to the sun and other thermal sources. The STOP model has two main control systems, one for line-of-sight (LOS) correction and an adaptive optics control system that uses a Shack-Hartmann sensor to control a deformable mirror. Combining information from multiple STOP models (one for each patch), a time-varying point-spread function (PSF) is computed. The relative positions of each cloud may vary with respect to each other, therefore an outer control system for maintaining precision phasing between the patches is necessary. In-focus PSF Optimizer (or "IPO") is another WFS&C algorithm developed at JPL for segmented optical systems. This sensor will drive the optical delay lines to maintain relative phase of each patch and will also feedback information to the LOS control to maintain pointing. Finally, the time-varying PSF is convolved with an image (or "scene"). Speckle imaging and multi-frame blind deconvolution algorithms are also being investigated to "clean up" the imagery to get an accurate estimate of the original scene.

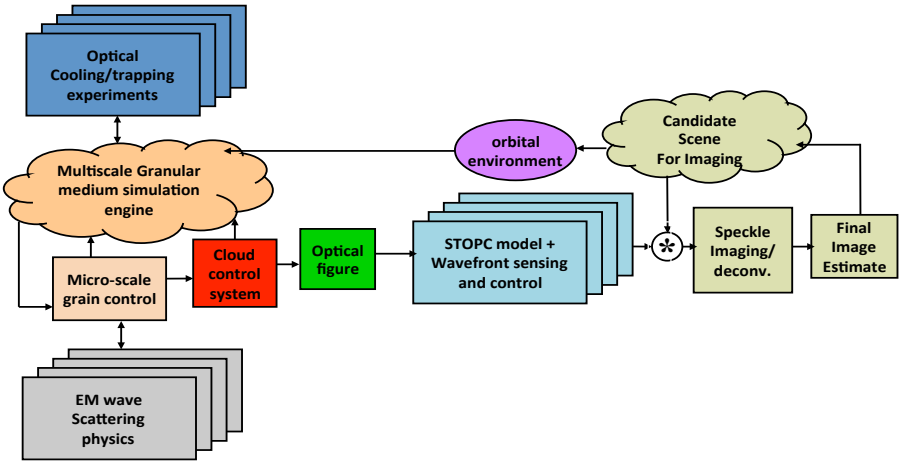

Figure 2. ***Granular Telescope Integrated Modeling Diagram***

III. Cloud Physics

Recent work [27] has investigated the feasibility of granular imaging system, concluding that such a system could be built and controlled in orbit. The accomplishments of our initial effort can be classified into four areas. Cloud-physics: gained initial insight into the physics of granular systems in space. Inside the cloud: developed an approach to deploy, contain, and align a cloud of reflective particles of the grain. Outside the cloud: designed optical imaging systems that include several layers of wavefront control to compensate for uncorrectable errors due to the stochastic nature of the cloud. Identified algorithms that reconstruct image estimates from an ensemble of incoherent images (e.g., multi-frame blind deconvolution). System-level: developed a preliminary multi-scale simulation, which predicts the time evolution of the imaging system kept in formation as it orbits the Earth. To address the engineering applications, we need to have insight on physics of disorder systems and the dominant forces that perturb the cloud. Related background can be found in refs [13], [19], [23]. Cloud gravito-electrodynamics leads to self-organization: for a cloud of particles released from an orbiting vehicle, the diffusion characteristics are important, as well as the tendency to form natural ring-like structures governed by the local gravity gradients, solar pressure, and radiation properties of each individual grain. The electrodynamic Lorentz coupling in LEO-GEO provides high degree of structural coherence which can be exploited in applicaitons. Once illuminated, the diffraction pattern from a disordered assembly leads to a strong focusing potential: the intensity of the signal is more collimated when the distribution of apertures is randomized, the separation between apertures increases, and the

number of apertures increases. Focusing is achieved by modulating the phase of the distributed radiators so as to obtain a conic phase surface, and this leads naturally to the shaping a cloud in the form of a lens. In space, the cloud behavior depends on the dynamic balance of different force fields: Laser light pressure, as light can induce motion; Solar illumination radiation pressure, which carries momentum; Gravitational forces and gradients, resulting in orbital and tidal effects; Electrostatic Coulomb or dielectrophoretic forces, since the grains are charged; Electromagnetic Lorentz forces resulting from the interaction with local magnetic field; Cloud self-gravity caused by the cloud being an extended body; Poynting-Robertson drag, in which grains tends to spiral down towards the Sun; and Yarkovstky (YORP) effect, caused by the anisotropic emission of thermal photons, which carry momentum. In the next sections, we describe the optical system analyses and the approach to control the system at the grain level, at the cloud level, and at the formation level.

A. Optical system analyses

Preliminary analyses have been carried out to compute the optical modulation transfer function (MTF) of the entire aperture as a function of spatial randomness, wavelength, fill factor, and other errors such as random tip and tilt of the grains, on the wavefront. These analyses provide insight on the positioning and stabilization requirements that need to be placed on the aperture. Some preliminary results are shown in Figures 3 through 6. Figure 3 shows plots of the random mask, generated without the exclusion process (so some overlap between grains can take place), compared to the filled aperture. Figures 3 to 6 show results of the random mask calculations with disks, ellipsoids, and aligned ellipsoids, generated with a Poisson exclusion process (non-overlapping grains), and fill factor = 5%, at a fixed wavelength. As expected, the shape of the grains is not very important, but the distribution, or fill factor, is. The next step would be to do sensitivity studies of the optical performance as a function of the various system parameters.

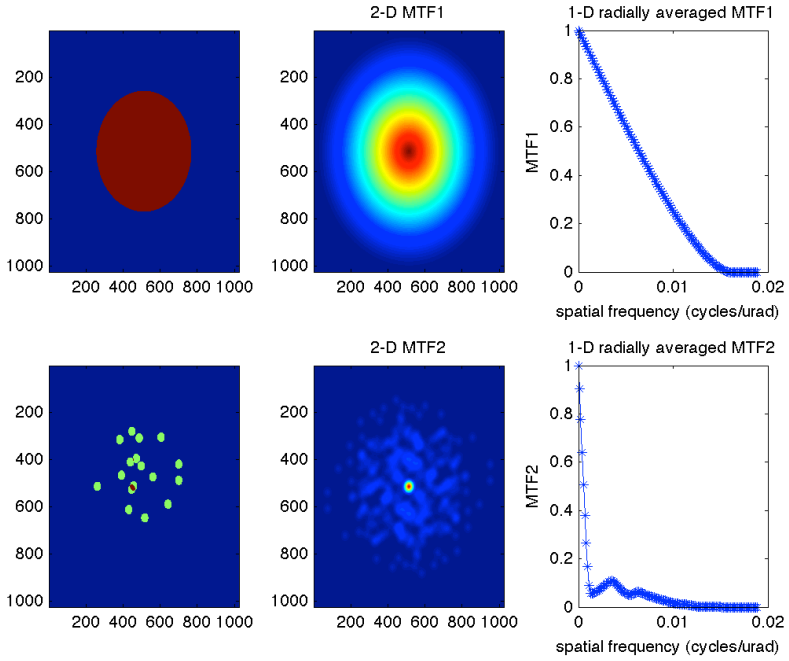

Figure 3. ***Plots on the random mask without the exclusion process compared to the filled aperture.***

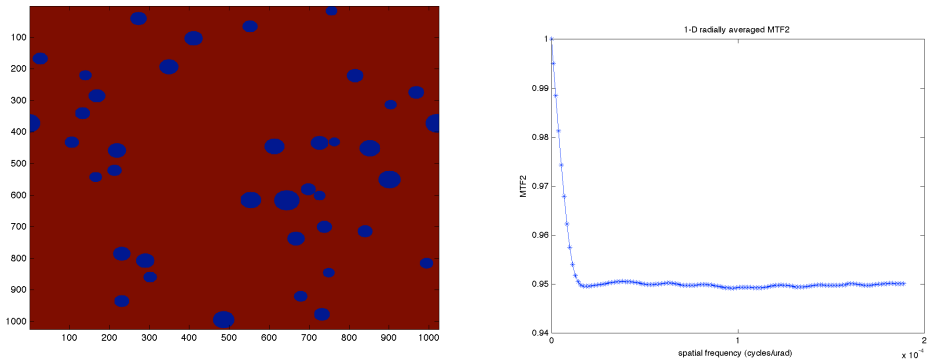

Figure 4. ***Plots on the random mask calculations with disks with Poisson exclusion process (non-overlapping grains), fill factor = 5%.***

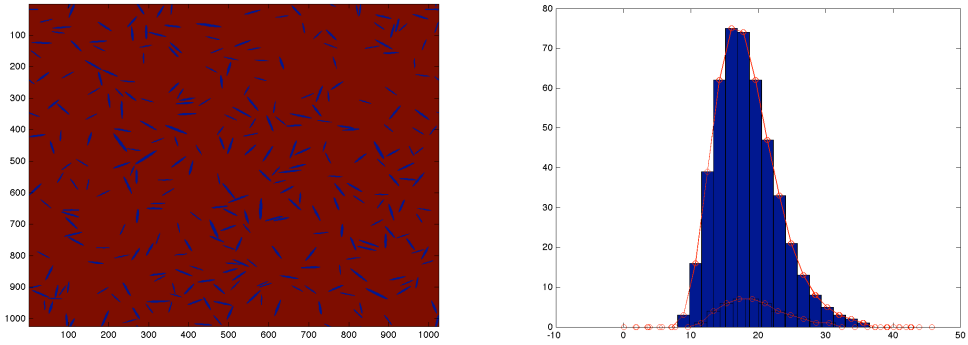

Figure 5. ***Plots on the random mask calculations with random needles with Poisson exclusion process (non-overlapping grains), fill factor = 5%, using a lognormal grain distribution (shown at right).***

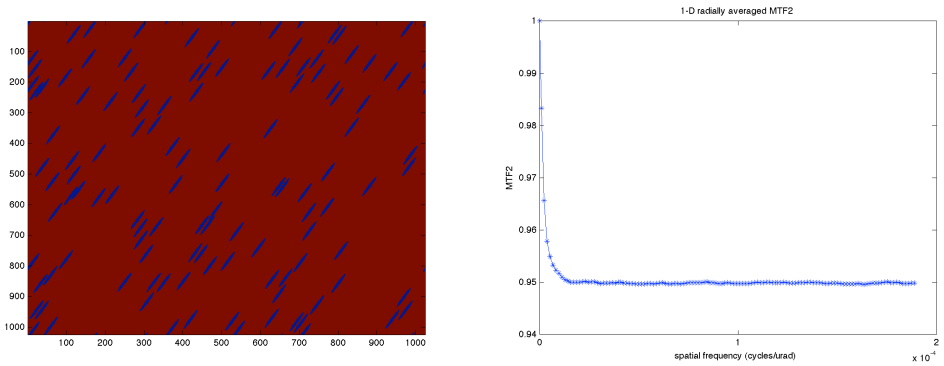

Figure 6. ***Plots on the random mask calculations with aligned needles with Poisson exclusion process (non-overlapping grains), fill factor = 5%.***

B. Control at grain level under uniform illumination

Dynamics and control of the cloud using laser beams requires knowledge of the position and orientation of the grains, and an understanding of how much error in position and orientation of the granular assembly can be tolerated before the imaging is not effective is necessary for telescope control. In this regard, at the large-scale, the imaging system is held in shape by means of formation flying technology. Established wavefront sensing and control techniques of adaptive optics are then used to stabilize the image assuming the granular aperture behaves as an equivalent monolithic aperture. We then invoke methods of sparse aperture technology, such as Golay arrays, to precisely formation-fly many clouds, which, at the microscale, are spatially random, but at the macroscale form a regular array. Through optical manipulation technology, we sense and control the average alignment of the grains within each cloud to provide a cloud figure shape that is adequate for our goals. Therefore, the top-down formation flying and adaptive optics approach merges with the bottom-up optical manipulation approach to achieve our goal to enable imaging scenarios.

Feedback control methodologies are being examined that can enable the three-dimensional guiding and stabilization of a single grain illuminated uniformly by a collimated monochromatic beam from a single direction.

The grain control law is derived to track a desired trajectory in grain alignment space as follows. The translation control actually implemented on the grain is of the form

$$\mathbf{f}_i = \mathbf{K}_p^{\,i}(\mathbf{q}_{Cmd}^{\,i} - \mathbf{q}_{Est}^{\,i}) + \mathbf{K}_v^{\,i}(\mathbf{v}_{Cmd}^{\,i} - \mathbf{v}_{Est}^{\,i}) + \mathbf{M}^i\mathbf{a}_{Cmd}^{\,i} \tag{1}$$

where $\mathbf{K}_p^{\,i}$ and $\mathbf{K}_v^{\,i}$ are translation control gain matrices, $\mathbf{M}^i$ is the grain mass matrix, $\mathbf{q}_{Est}^{\,i}$ and $\mathbf{q}_{Cmd}^{\,i}$ represent the estimated and commanded translation state, respectively. The rotational control instead is of the following form

$$\mathbf{t}_i = \mathbf{\Gamma}_p^{\,i}(\mathbf{l}(q_{err})_{Cmd}^{\,i} - \lambda\,(q_{err})_{Est}^{\,i}) + \mathbf{\Gamma}_p^{\,i}(\mathbf{w}_{Cmd}^{\,i} - \mathbf{w}_{Est}^{\,i}) + \mathbf{J}^i\mathbf{a}_{Cmd}^{\,i} \tag{2}$$

where $\mathbf{\Gamma}_p^{\,i}$ and $\mathbf{\Gamma}_v^{\,i}$ are rotational control gain matrices, $\mathbf{J}^i$ is the grain moment of inertia matrix, λ is the eigenaxis of rotation, θ_{err} is the magnitude of rotation corresponding to the difference between the commanded and the estimated quaternions, and **w** and **a** are the grain angular velocity and acceleration respectively.

The effect of the laser illumination on the grain can be quantified by an "optical efficiency" gain G=A I r/c, where A is the grain frontal area (exposed to light), r is the grain radius, I is the light intentity in [W/m2], c is the speed of light in vacuum. Defining by α=acos(n*U) as the grain "angle-of-attack" [Schuster, 2014] to the illumination direction U, and n the normal vector to the grain reflective surface, the optical forces on the grain are:

$$\begin{aligned} Fx &= 0 \\ Fy &= G*Qy(\alpha) \\ Fz &= \sin(\alpha)*Qz(\alpha) \end{aligned} \tag{3}$$

and the optical torques are:

$$\begin{aligned} Tx &= \sin(\alpha)*Qx(\alpha) \\ Ty &= 0 \\ Tz &= 0 \end{aligned} \tag{4}$$

where the optical efficiency values are interpolated from the values in Figure 7, obtained from analys done with a commercial geometric ray-optics program.

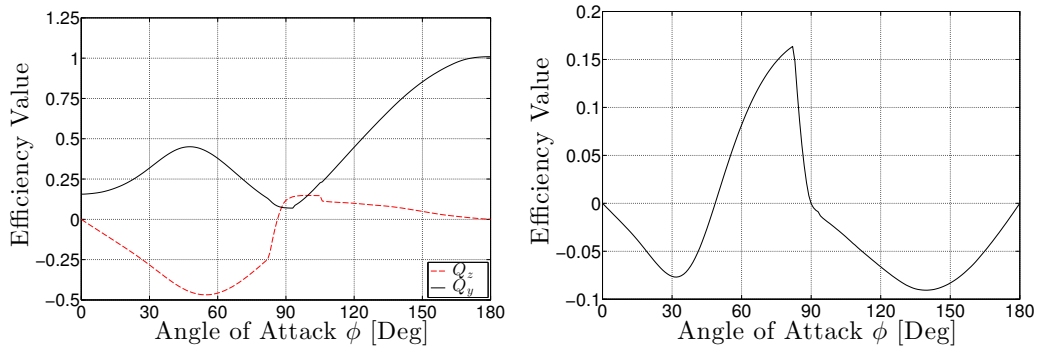

Figure 7. ***Radiation force and torque efficiency tables, as a function of grain angle-of-attack, from [Schuster, 2014].***

Figure 8 shows the results of simulated three-dimensional attitude control of grain guided from +30 degrees to -30 degrees in pitch by one uniform collimated beam (frv= angles, therr=angular error, werr=angular rate error, aoa=angle of attack, aoad=rate of angle of attack, f=control force, tau = control torque, bottom right plot is irradiance). These results indicate that one degree of freedom is fully controllable with arbitrary precision with a feedback plus feed-forward control architecture that senses the angle-of-attack of the grain (angle between the normal to the mirror plane and the illumination direction). This is similar to the optical-tweezer feedback, which however, is done in a medium. Therefore, we are exploring the options offered by control for optical tweezers and how much of the existing techniques can be extrapolated for operation in a vacuum, in the absence of a medium.

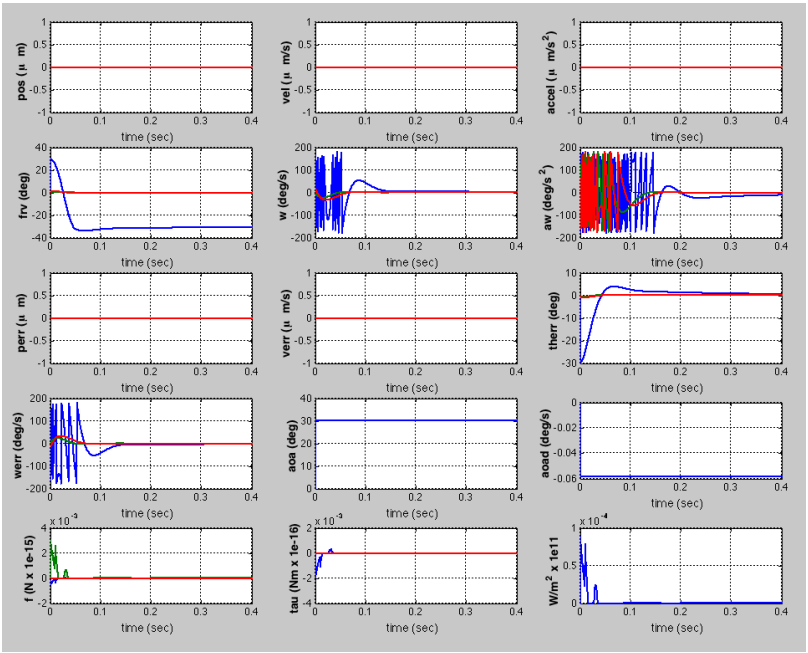

Figure 8. ***Results of simulated 3D attitude control of grain guided from +30 degrees to -30 degrees in pitch by one uniform collimated beam (frv= angles, therr=angular error, werr=angular rate error, aoa=angle of attack, aoad=rate of angle of attack, f=control force, tau = control torque, bottom right plot is irradiance).***

IV. Proposed Wavefront Control Architecture for Granular Sparse Aperture Telescope

A granular sparse aperture telescope (GSAT) is a space-borne imaging system that makes use of a collection of small reflective grains to form a sparsely filled primary mirror. The GSAT concept is depicted graphically in Figure 9. A cloud of reflective grains are constrained into a parabolic shape to form a primary mirror. Light reflected from each grain is now focused into a back-end system consisting of a control system and detector. Compared to monolithic mirrors, a GSAT will be extremely light-weight and will also allow for much larger aperture sizes. As stated above, in the current design, the "cloud" of grains will be shaped roughly into a parabolic shape by a space-borne optical trap [see Fig. 9]. However, in order to be an effective imager, the wave-fronts reflected from the parabolic surface of the cloud must be corrected in order to form a useful point spread function. In this section, we outline the details of a proposed control system that may be used in conjunction with the optical trapping system to correct the wave-fronts so that the GSAT will generate high resolution image that fully realize the potential of larger aperture sizes.

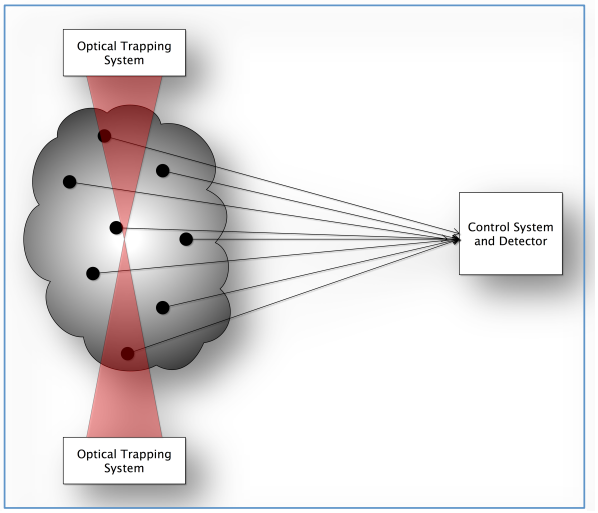

Figure 9. ***A granular sparse aperture telescope.***

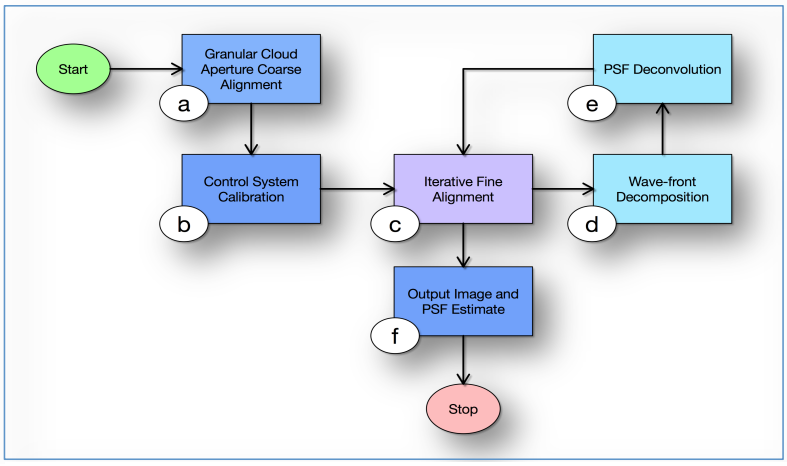

Figure 10. ***The granular cloud aperture wave-front control process.***

The wave-front control process for the GSAT is depicted in Figure 8. The wave-front control process begins by first coarsely aligning the cloud grains into a parabolic shape by using an external trapping force [Fig. 10 (a)]. The coarse alignment system must be able to shape the granular cloud enough so that the reflected light from all grains falls upon the system's detector. Next we must prepare our control system to correct the incoming reflected E-field [Fig. 10 (b)]. Typically, a control system will correct the E-field by applying a field correction that cancels the error when the field is compared to an ideal field:

$$E_{correction} = -(E_{aberrated} - E_{ideal}) \tag{9}$$

The control system applies this correction by altering the phase or amplitude of the incoming field (typically the phase) in such a way as to induce the correction. For example, a deformable mirror (DM) is a common optical control device that's shape may be in order to apply the correction given in Equation 9. The difficulty lies in sensing what correction is needed! Traditionally this was accomplished by directly measuring the field (phase, amplitude, or both) in the pupil plane (typically the same plane as the primary mirror). However this is not strictly necessary. What is necessary is that you know how the system's final image plane field is affected by your control parameters. In the case of a deformable mirror, you have control over the surface height of the actuators that are used to shape the mirror. So now you just need to actuate your control device and see how the final image is affected. However, it is important that your control parameters form an orthogonal basis set, or can be actuated independently. To calibrate our control system [Fig. 10 (b)], we first need create an orthogonal set of control states and then actuate each one and determine the effect on the final image plane field. There are multiple ways to do this but for brevity I'll describe three germane methods. The first method is Move Each Grain – Each grain may be moved independently (ideally, perpendicular to the Pupil plane of the telescope. This is the most direct set of control states, however they are also the hardest to control since it requires physically moving each grain. The second method is Image the Pupil onto a DM. You may image the pupil onto a DM and then actuate each actuator in the DM. This is much closer to a standard wave-front control method, however it requires you to image the cloud of grains onto a deformable mirror, which adds complexity. Also the capture range (maximum wave-front correction) of standard DMs may not be sufficient for our purposes and a more exotic DM may be required. The thirst method is Perturb the Cloud – Another possible method is to apply orthogonal disturbances to the cloud via the optical trapping system. You can apply different orthogonal forcing functions to the trap such as different frequency sine waves. In this case, we don't need to image the pupil or move the grains directly. For this reason this is an attractive method, but is also the least understood and must be further investigated. Now we can form a gain matrix (G) that describes how actuations of our control system ($S_{control}$) change our image plane field (dE_{image}):

$$dE_{image} = G * S_{control} \tag{10}$$

Using a pseudo-inversion method, we may invert the gain matrix and now determine the state of our controller that will yield the desired change to our image plane E-field:

$$S_{control} = G^{-1} * dE_{image} \tag{11}$$

Now we iteratively correct the field [Fig. 10 (c)]. During each iteration we apply equation 3, [Fig. 10 (d)] to determine a field correction. As a second step we may also use our knowledge of the grain PSF to perform a PSF de-convolution [Fig. 10 (e)]. This may reduce the number of iterations needed for conversion. After we have obtained the desired PSF or image quality [Fig. 10 (f)], we may now maintain the system periodically while imaging.

V. Granular imager dynamics and control

This section follows the approach for formation dynamics and control presented in [16] and in [21]. The

Granular Telescope formation most basic active elements are five free-flying optical modules. The free flyers are

- S0, the primary mirror cloud (PMC)
- S1, the free flying mirror (FFM)
- S2, the Focal Plane Assembly (FPA)
- S3, The Primary Figure Sensor (PFS)
- S4, the Laser Containment/Trapping System (LCTS)
- S5, the co-orbiting sunshade (OSS)

The following assumptions are used in this report:

- The formation is composed of five rigid bodies (sunshade dynamics is neglected).
- The orbit is circular.
- The formation dynamics is described (and numerically integrated) with respect to the Orbiting Reference Frame, to be described next.

C. Reference Frames

- F_I - Inertial Frame F_I taken as J2000
- F_C - Define the PMC frame F_C by 3 fiducial points at the periphery of the PMC membrane. The z axis is defined normal to the fiducial plane, and in the direction of the nominal LOS of the telescope. The F_C frame is located at the "mechanical center" of the PMC, defined by the mean location of the three fiducial points.
- F_O - Define the Orbital frame F_O of the PMC for a geosynchronous or heliocentric orbit. The orbital frame is defined with x_O axis along positive radial vector r from Sun center to the mechanical center of the PMC, and z_O=rXv, where v is the orbital velocity vector. The orbital frame is assumed to be located at the mechanical center of the PMC.
- F_T - Telescope Formation Frame F_T, is an inertial frame located at center of PMC, which specifies the desired attitude of the telescope (this points the telescope LOS to a desired J2000 location, and maintains acceptable twist angle of the formation).Thus defined, the z axis of F_T, is labelled as the axis of the desired telescope LOS.
- Define body frames F_fpa, F_pfs, and F_lcts for the free flying elements FPA, FPS, LCTS, respectively.
- q_A - Define the formation attitude q_A as the quaternion (or equivalent direction cosine matrix A) which maps the F_I frame into the F_T frame, i.e., F_T= A F_I
- q_R - Define the PMC alignment as the quaternion q_R (or equivalent direction cosine matrix R) which maps the F_T frame into the F_C frame, i.e., F_C=q_R F_T

D. Assumptions for Dynamics

The assumptions we used to model the dynamics are as follows: 1) The inertial frame F_I is fixed at Earth's center. 2) The orbiting Frame (ORF) F_O follows a Keplerian orbit. 3) the cloud system dynamics is referred to F_O. 4) the attitude of each grain uses the principal body frame as body fixed frame. 5) the atmosphere is assumed to be rigidly rotating with the Earth. Regarding the grains forming the cloud: 1) each grain is modeled as a rigid body; 2) a simple attitude estimator provides attitude estimates, 3) a simple guidance logic commands the position and attitude of each grain, 4) a simple local feedback control of local states is used to stabilize the attitude of the vehicle. Regarding the cloud: 1) the cloud as a whole is modeled as an equivalent rigid body in orbit, and 2) an associated graph establishes grain connectivity and enables coupling between modes of motion at the micro and macro scales; 3) a simple guidance and estimation logic is modeled to estimate and command the attitude of this equivalent rigid body; 4) a cloud shape maintenance controller is based on the dynamics of a stable virtual truss in the orbiting frame. Regarding the environmental perturbations acting on the cloud: 1) a non-spherical gravity field including J0 (Earth's spherical field) zonal component, J2 (Earth's oblateness) and J3 zonal components is implemented; 2) atmospheric drag is modeled with an exponential model; 3) solar pressure is modeled assuming the Sun is inertially fixed; and 4) the Earth's magnetic field is model using an equivalent dipole model. The equations of motion are written in a referential system with respect to the origin of the orbiting frame and the state is propagated forward in time using an incremental predictor-corrector scheme.

Figure 11 shows the kinematic parameters of a 1000 element cloud in orbit. The motion of the system is described with respect to a local vertical-local horizontal (LV-LH) orbiting reference frame (x,y,z)=F_{ORF} of origin O_{ORF} which rotates with mean motion Ω and orbital semi-major axis R_0. The orbital geometry at the initial time is defined in terms of its six orbital elements, and the orbital dynamics equation for point O_{ORF} is propagated forward in time under the influence of the gravitational field of the primary and other external perturbations, described below. The origin of this frame coincides with the initial position of the center of mass of the system, and the coordinate axes are z along the local vertical, x toward the flight direction, and y in the orbit normal direction. The inertial reference frame (X,Y,Z)=F_I is geocentric inertial for LEO (X points toward the vernal equinox, Z toward the North Pole, and Y completes the right handed reference frame), and heliocentric inertial for other applications. The orbit of the origin of F_{ORF} is defined by the six orbital elements a (semimajor axis), e (eccentricity), i (inclination), Ω_L (longitude of ascending node), w (argument of perigee), ν (true anomaly), and time of passage through periapsis. From Figure 9, the position vector of a generic grain with respect to O_{ORF} is denoted by $\boldsymbol{\rho}_i$, and we have $\mathbf{r}_i=\mathbf{R}_0+\boldsymbol{\rho}_i$. We define the state vector as

$$\mathbf{X}=\left(\mathbf{r}_E,\dot{\mathbf{r}}_E,\mathbf{R}_0,\dot{\mathbf{R}}_0,\ldots\rho_i,\mathbf{q}_i,\dot{\rho}_i,\omega_i,\mathbf{R}_s,\dot{\mathbf{R}}_s,\rho_s,\dot{\rho}_s,\mathbf{q}_s,\omega_s\right) \tag{1}$$

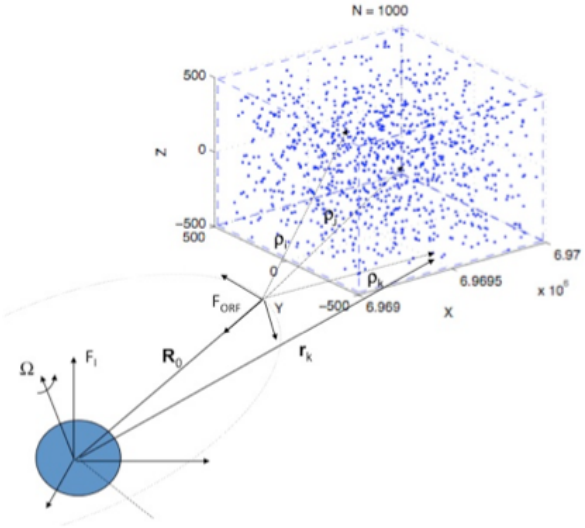

Figure 11. ***Geometrical description of orbiting cloud in orbit.***

where $\mathbf{q}_i$ and $\boldsymbol{\omega}_i$ represent the quaternion and angular velocity vector of the i-th grain with respect to F_I. The translation and rotation kinematics at the grain level are:

$$\text{grain}\begin{cases}\mathbf{V}_0=\dot{\mathbf{R}}_0\\ \mathbf{v}_i=\dot{\rho}_i\\ \dot{\mathbf{R}}_{bi}=-\omega^{\times}\mathbf{R}_{bi}\end{cases}\qquad\text{cloud}\begin{cases}\mathbf{V}_s=\dot{\mathbf{R}}_s\\ \mathbf{v}_s=\dot{\rho}_s\\ \dot{\mathbf{C}}_{si}=-\omega_s^{\times}\mathbf{C}_{si}\end{cases} \tag{2}$$

The angular momentum balance is:

$$\begin{aligned} &\textbf{grain} \quad \mathbf{J}_i\dot{\omega}_i + \omega_i^{\times}\mathbf{J}_i\omega_i = \sum_{j=1}^{Npert}\tau_j \\ &\textbf{cloud} \quad \mathbf{J}_s\dot{\omega}_s + \omega_s^{\times}\mathbf{J}_s\omega_s = \tau_s \end{aligned} \tag{3}$$

and the linear momentum balance is:

$$\textbf{grain}\begin{cases} \dot{\mathbf{V}}_0 = -\mu_E\dfrac{\mathbf{R}_0}{\left|R_0\right|^3} + \dfrac{\sum_{j=1}^{Npert}\mathbf{f}_j}{m_{total}} \\ \ddot{\rho}_i = -\dot{\mathbf{V}}_0 - \dot{\Omega}^{\times}\rho_i + \Omega^{\times}\Omega^{\times}\rho_i - 2\Omega^{\times}\dot{\rho}_i + \mathrm{A}_i\ddot{\mathbf{r}}_i \\ \ddot{\mathbf{r}}_i = -\mu_E\dfrac{\mathbf{r}_i}{\left|\mathbf{r}_i\right|^3} + \dfrac{\left(\mathbf{f}_a + \mathbf{f}_e\right)_i}{m_i} \end{cases} \qquad \textbf{cloud}\begin{cases} \dot{\mathbf{V}}_s = -\mu_E\dfrac{\mathbf{R}_s}{\left|R_s\right|^3} + \dfrac{(\mathbf{f}_{J2} + \mathbf{f}_{J3})_s}{m_s} \\ \ddot{\rho}_s = -\dot{\mathbf{V}}_s - \dot{\Omega}^{\times}\rho_s + \Omega^{\times}\Omega^{\times}\rho_s - 2\Omega^{\times}\dot{\rho}_s + C_{si}\dfrac{\mathbf{f}_s}{m_s} \end{cases} \tag{4}$$

where: A_i= rotation matrix of i-th body frame wrt. Inertial; R_0= orbital radius vector to origin of ORF; Ω = orbital rate; C_{si}= rotation matrix of cloud body frame wrt. Inertial; $f_{a,e}$ = actuation + external forces (gravity, aerodynamics, magnetic, solar); $m_{i,s}$ = grain/cloud mass; $w_{i,s}$ = body, cloud angular rate; $\tau_{a,e}$ = actuation + external torques; $J_{i,s}$ = grain/cloud moment of inertia.

E. Formation Control Model

The Granular Imager Control diagram is shown in Figure 12. This is a functional description of the control and estimation algorithms involved in the Granular telescope formation dynamics. Once the commands to reshape the formation have been issued to each element in the formation, the formation estimator determines the inter-spacecraft relative distabce and bearing. This information is passed to the formation guidance planner, which sends inputs to the attitude and position controller of each spacecraft. Each spacecraft is controlled by a reaction wheel and thruster control logic, and requires ephemeris data to know its position along the orbit. The sensors on-board each spacecraft provide state information that is used in the attitude and formation estimator to predict the dynamics.

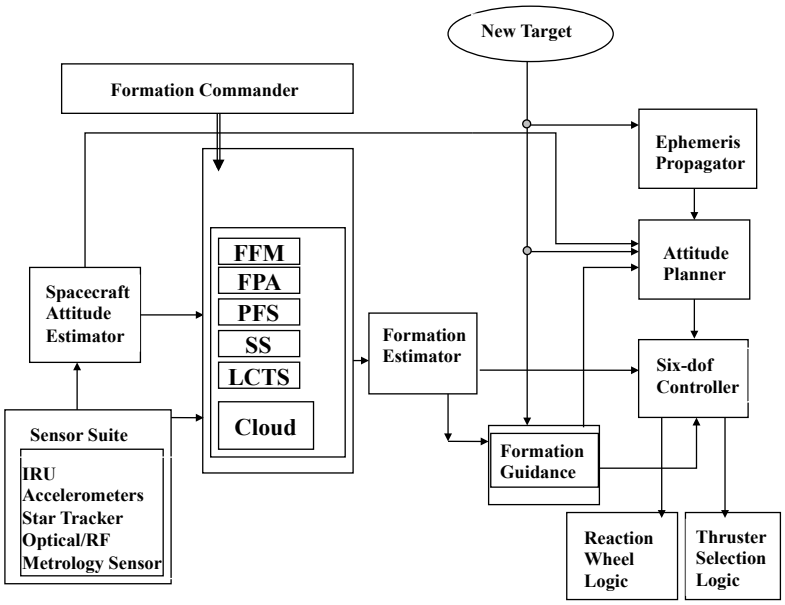

Figure 12. ***Granular Telescope Formation Command & Control Functional Diagram.***

F. Formation Guidance Model

With S_0 at the origin of the coordinate frame defined by the axes (T, C, N), and ignoring the OSS for the time being, the relative coordinates of S_i,, i=1, …, 5 at the initial time were chosen to be as in Figure 13, where (p_i, q_i, r_i) are the formation coordinates of the S_i. The coordinates above define a virtual formation that is to be maintained throughout the flight. Figure 13 depicts the bird-eye view of looking down at the C-axis. S_0 is allowed to translate freely along the T, C, and N axes, and also to sway about the C-axis, which induces an anti-clockwise rotation θ_y. In order to maintain the same relative position of the Granular Telescope formation, each free flyer S_i therefore has to move along with the translational motion of S_0, and also to translate from the solid circular position to the dotted position as shown in Figure 13 to compensate for the angular rotational of S_0. Note that in Figure 13 L_i is the projection of the line joining S_0 and S_i on the (TN)-plane; S_0 and S_i may actually have different coordinates in the C-axis.

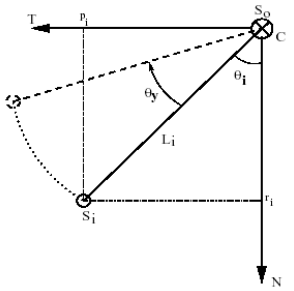

Figure 13. ***Depiction of intended retargeting slew in orbital plane.***

G. Formation Measurements

Figure 14 shows a proposed architecture for the Granular Imager Formation Laser and RF Metrology Systems. The RF metrology subsystem collects from each formation element receiver data of range and phase, at each of 3 antennae, of signals from a transmitter on each other element. This is a set of 6 one-way links for each element pair. The 6 links provide an RF "truss" to determine the relative position and attitude of the two elements. Assuming that all the common errors in the system have been calibrated (or solved for) and attitude is known accurately from Attitude Estimation, each "truss" can be viewed as an independent measurement of the relative position of the two elements. Previous analysis has shown that the measurement accuracy can be characterized by independent range (along the LOS) and bearing (2 dof pointing normal to the LOS) errors. Simulation of the RF metrology subsystem can be carried out on two levels, simulating individual RF links as input to an extensive processing algorithm or simulating the outputs of the process, the equivalent "truss" measurements. The latter is more suitable for a higher level system functional simulation where the subsystem low level detail is not important.

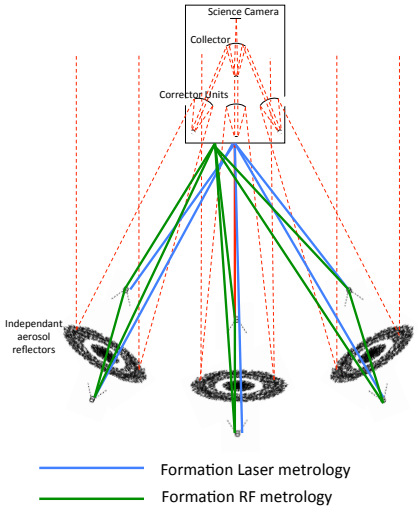

Figure 14. ***Proposed architecture for Granular Imager Formation Laser and RF Metrology Systems.***

H. Formation Estimator

A proposed block diagram for the Granular Imager Formation Estimator is shown in Figure 15. An estimator of the formation relative state is needed both in simulations as well as in real life because the control of the formation rigidity demands an accurate knowledge of the relative range and range rate between adjacent spacecraft. In this section we deal with the relative translation estimator only. The current implementation of the translation estimator estimates only the relative position and velocity of adjacent spacecraft. This implies that the measurements used depend only on relative position and are not correlated to other system variables such as the attitude estimates of the spacecraft, or the misalignments between various subsystems. This assumption is acceptable only as long as the effects of these secondary disturbances are small compared to the errors in the relative position measurements (e.g. attitude estimate error is much less than metrology bearing measurement uncertainty). The metrology measurements are also assumed to be independent and uncorrelated between measurements, which implies that any common factor within the metrology subsystem have been removed, by calibration or estimation, in the internal processing. The radio-frequency metrology subsystem collects from each formation element receiver data of range and phase, at each of three antennae, of signals from a transmitter to three receivers on each element. This represents six one-way links for each element pair. These six links provide an RF "truss" to determine the relative position and attitude of the two elements. After measurement and estimation, the following input data is available to the Commander/Controller of the formation. For each spacecraft, we have: linear position, velocity, acceleration vectors, quaternion, angular velocity, angular acceleration vectors in relative bearing and bearing rate, relative range and range rate, all measured with respect to the vehicle's body frame, the neighbor spacecraft body frame, and the inertial frame. The estimation of the attitude of each spacecraft is decentralized. Star tracker and gyro measurements are each spacecraft are processed to give the spacecraft attitude relative to an inertial frame. Accelerometer and relative position measurements in the form of an RF metrology sensor are also available.

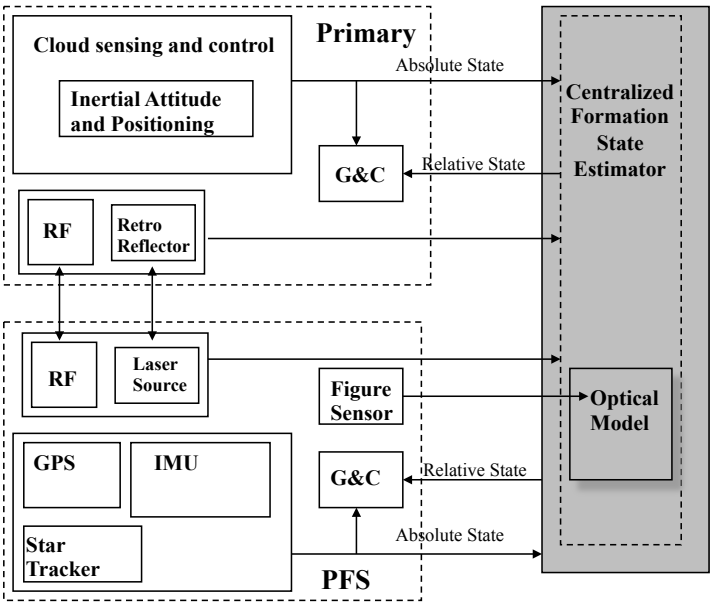

Figure 15. ***Granular Telescope Formation Estimator***

VI. Application to Control of a Representative Optical Imaging System

Resolution and aperture sizes for astrophysical optical systems are ever increasing in demand [14], [16]. With near-term plans to build 30 meter ground-based telescopes for astronomy, the demand for higher resolution optics in space continues to grow not only for exo-planet detection, but also for earth-based science, including hyper-spectral imaging and for monitoring of the oceans and land masses (e.g. seismic monitoring). ATLAST, still several decades away, is the largest practical space telescope designed using state-of-the-art light-weight segmented mirror technology: it may have an aperture up to 18 m. The aperture formed by the granular spacecraft cloud does not need to be continuous. Used interferometrically, for example, as in a Golay array [4], imagery can be synthesized over an enormous scale. As part of our investigation, we have considered refractive, reflective and holographic systems and outlined optical correction and collection systems. In addition to forming a single monolithic optical element with the cloud, we also considered forming smaller self-coherent patches, similar to segments in a segmented aperture, but not required to be phased with respect to each other. The "segments" can be continuous or separated by large amounts to form a sparse array. A corrector is then used to compensate for phase differences between each "segment". A Fizeau interferometer is a straightforward corrector for a reflective system. A more advance corrector would be a multiple aperture system utilizing multi-scale lens design, as described by [4]. The multi-scale lens design has the additional benefit of an increased field of view of the optical system and will allow for less movement of the entire collection of sub-apertures when changing the line of sight of the system.

An optical imaging system design has been selected as the best candidate architecture for a space system involving a cloud. The concept design is shown in Figure 16. The sequence of optics is as follows: the starlight is focused by granular spacecraft optic "patch", creating a spherical wavefront. Light from all patches converges at an intermediate focus, which has an image-plane coded aperture. The light then reflects off secondary mirror (Gregorian) and the light from each patch is collimated. Each beam goes to a separate adaptive optics system. A fast steering mirror and a deformable mirror correct pointing and low to mid-spatial frequency aberrations. An optical delay line is used to correct phasing difference between the patches and allow for Fourier transform spectroscopy. A beam-splitter is included to allow some of the light to go to a Shack-Hartmann sensor to measure aberrations in the system. For this system, the selected approach for cloud management/sensing/control is multistage, with an outer stage for formation stabilization, and an inner stage for telescope wavefront sensing and correction, relegating fine adaptive optics to a deformable/fast steering mirror stage in the optical bench. The system's relative range/bearing sensing and metrology is based on virtual telescope formation flying, in which distributed relative sensing is

accomplished using Ka-Band transceivers/patch antennas, and a centralized laser metrology system, relying on a single laser source on the main light-collecting spacecraft, while single reflecting target are on other free-flying elements except granular spacecraft.

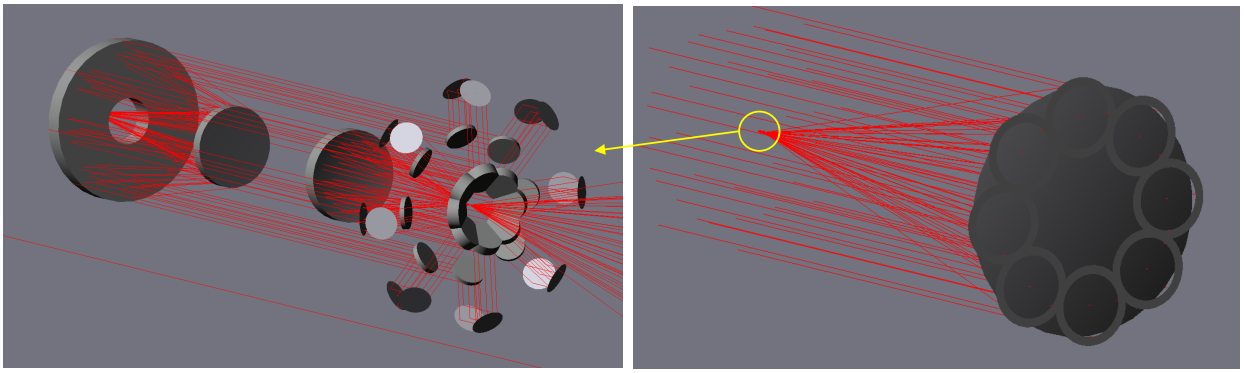

Figure 16. ***Reflective imaging system concept design with 8 cloud patches forming the aperture.***

The cloud sensing approach is based on imaging/laser scanning, relying on custom or commercial stereo vision or laser scanning systems which can create precise 3-D model of complex objects. The approach for cloud control is multistage, based on laser cooling, and involves three levels: a) Trapping ("corralling") through gradient forces to provide containment against cloud diffusion due to thermal, radiation, and gravity and cloud cooling; b) shaping/alignment through laser pressure, to change amorphous cloud into disk or rectangular carpet; and c) alignment of grains to wavefront direction, which implements wavefront/boresight control through adaptive optics in order to maintain optical figure. Related work is presented in [2], [10], [11], [14]. For any size/shape particle, the electromagnetic energy is minimized when the particle is in the brightest region of the laser beam, and this is the basis for light-induced control. Corralling assumes mechanically releasing the cloud with low ejection velocities, then applying 3-axis laser illumination to corral the cloud via optical gradient forces. The cooling approach can be achieved by means of gradient forces, which involves rotating the linear polarization direction of the control laser at the rocking frequency. This effectively freezes the oscillations in a rotating reference frame. By adiabatically slowing the rotation of the polarization axis, some population of particles can be made to assume the same orientation, e.g., with the flat mirrored side of the rod facing the center of curvature. Cloud shaping is carried out via raster scanning of the beam across granular patch. An optimization is needed of the time dependent beam power and beam velocity to capture the most particles, and will be subject of future work. Grain alignment for phase coherence is achieved by applying linearly polarized control laser to orient particles along dominant polarization axis (long axis of rod), so that the particles will rock under the influence of polarization torque and radiation pressure torque.

A representative cloud with varying number of grains is simulated to identify the limitations in computation time as the number of grains grows. We can derive a control law to track a desired surface in the ORF (equivalently to maintain a reference cloud shape) as follows [15], [21], [22]. Define the tracking error $e_Z = q(x,y) - q_d(x,y)$, where $q_d(x,y)$ are the desired surface, and $q(x,y)$ the current position of the grain belonging to that surface with respect to the origin of ORF. By imposing an exponentially stable error dynamics in the form $\ddot{e}_Z + 2\zeta_Z \omega_Z \dot{e}_Z + \omega_Z^2 e_Z = 0$, we can make sure the error e is driven to zero. Therefore, using the equations of motion expressed in ORF coordinates, the feedback-feedforward control law with components in ORF becomes:

$$u = -f_{pert} + f_{gyro} + m\ddot{q}_{des} - K_d \dot{e} - K_p e \,. \qquad (13)$$

where f_{pert} is the resultant of the gravitational forces on the grain, f_{gyro} are the Coriolis and centrifugal forces acting on the grain, Kd is a derivative gain, and Kp is a proportional gain. Both f_{pert} and f_{gyro} can be modeled, act on a time scale which is very long, and can be canceled out by the feed-forward control scheme. These control forces are applied by the laser scanning system, coupling mechanically with the grains via opto-mechanical interaction.

We envision a multi-stage approach for the assembly and containment of the aperture. See Figure 17. First, the cloud is deployed. In the 1980's, AMPTE (a prior NASA mission of upper atmospheric aerosol investigation) released sodium aerosol in the ionosphere. The cloud then needs to be trapped to avoid leakage and diffusion. A pair of counter-propagating laser beams could trap the cloud at the interference fringe, as originally proposed in [Labeyrie].

Once the cloud is trapped, we need a coarse control stage to create a roughly two-dimensional carpet from the cloud. Besides using light pressure, magnetic or electrostatic field might help this process. The carpet does not need to involve the entire cloud, only part of it. Once we have the carpet, we need a fine control stage for figure control. The approach involves the use of tight, large-scale, formation flight technology for precision alignment of the cloud aperture with the remaining optical system elements, but specific optical lift technology for coarse and fine cloud control and shaping. Electrostatic charging might cause undesired aggregation and clustering that might counteract the optical lift force. For this reason, combinations of optical, magnetic, electric, and gravitational forces will have to be considered to control and manipulate the cloud. The cloud will experience very small gravity gradient forces if deployed at a Lagrange point (for example, the Sun-Earth L2 point), which will not disrupt the cloud's stability over time, and only infrequent orbital correction maneuvers would be necessary to maintain the system in orbit. Once the observation campaign is over, the system can be decommissioned, and the same force fields can be used to de-orbit the cloud, or used advantageously to clean other orbital debris.

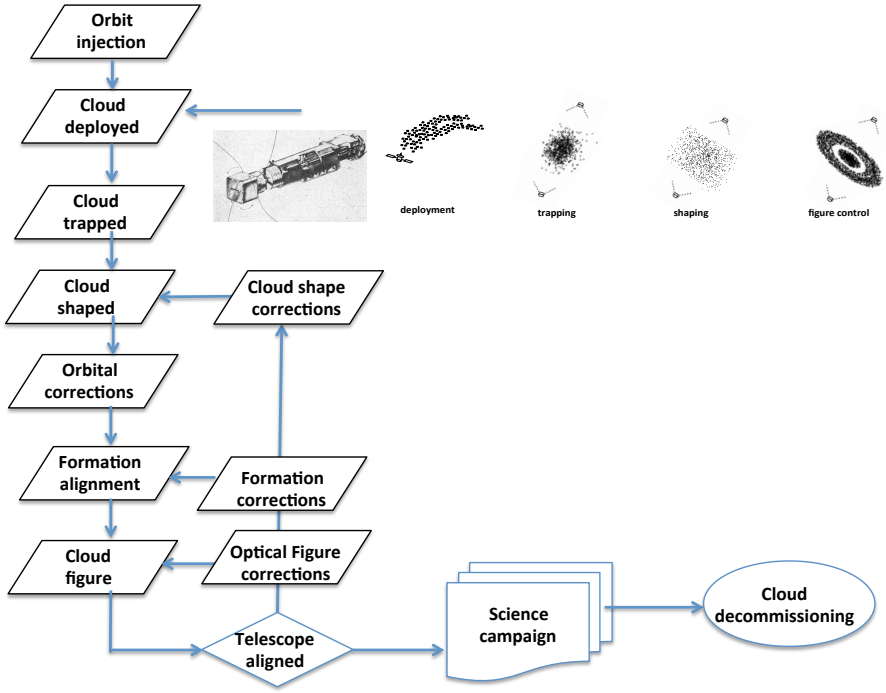

Figure 17. ***Granular Telescope Deployment and Operations***

VII. Theoretical Developments for Radar Tomography

We are developing radar instrument architectures that use cloud physics and scattering to enable tomographic imaging in previously inaccessible areas of bodies (comets, asteroids) - Rayleigh or small particle approximations is used to model cloud physics. The problem of using granular media to aid in microwave imaging requires the study of two general bodies of problems. The first general problem involves the vector radiative transfer theory to describe the exact phase sensitive scattering of incident waves by the granular medium, which may be complex in nature with various particle sizes, distributions, and dielectric and conductive properties. The second general problem involves the exact image inversion theory based on phase sensitive scattering of a general distributed scene to be imaged –

which may also contain various inclusion/target sizes, distributions, and dielectric and conductive properties. These two problems can be somewhat decoupled to permit development of each independent of the other. To avoid undue and unnecessary complications, the approach has been to limit the problem to two-dimensions and to use cylindrical media for both the granular medium constituents and the targets in the imaging scene. To permit coherent imaging of the target with aid from the granular media in directing energy, both problems must permit multiple scattering and complex dielectric properties to allow volume currents inside the media, as opposed to just surface scattering found from perfect conducting mediums.

The first problem has been recently addressed using a boundary value method to account for multiple scattering from particles using various sizes, distributions, and complex permittivity values. This approach decomposed the problem into transverse electric (TE) and transverse magnetic (TM) wave components, and solves the boundary conditions for each cylindrical particle using the usual boundary conditions, and it is shown in Figure 18. Presented in a T-matrix solution, the technique permits efficient calculations of the exact plane-wave scattering of TE and TM waves by the arbitrary granular media. The second problem is being addressed using a similar technique. The scattered field is computed in a similar manner, but instead of calculating the scattering of the granular media, we calculate the scattering of the target scene. This scattered wave solution is then used to form an image using the time-domain back-projection technique, which projects scattered fields in time into specific pixels within the imaging plane in a coherent manner. Figure 19 shows an example of reconstructed image from three sensors. To simplify the current development, we use back-scatter from the target scene – therefore describing a mono-static microwave radar problem. The exact scattering permits use of various properties and configurations of the scene to be imaged. As an example, the image below (Figure 20) shows a small collection of four targets being imaged using coherent and incoherent versions of the time-domain back-projection inversion. The particles are of different sizes and the image-plane is shown for particles that have properties of ice, pure water, salt water, and the ideal target case of perfect conductors. Even in this simple example, we see the artifacts of scattering in the image due to low-loss dielectrics. Coherent imaging is shown to reduce these artifacts considerably when compared to incoherent imaging.

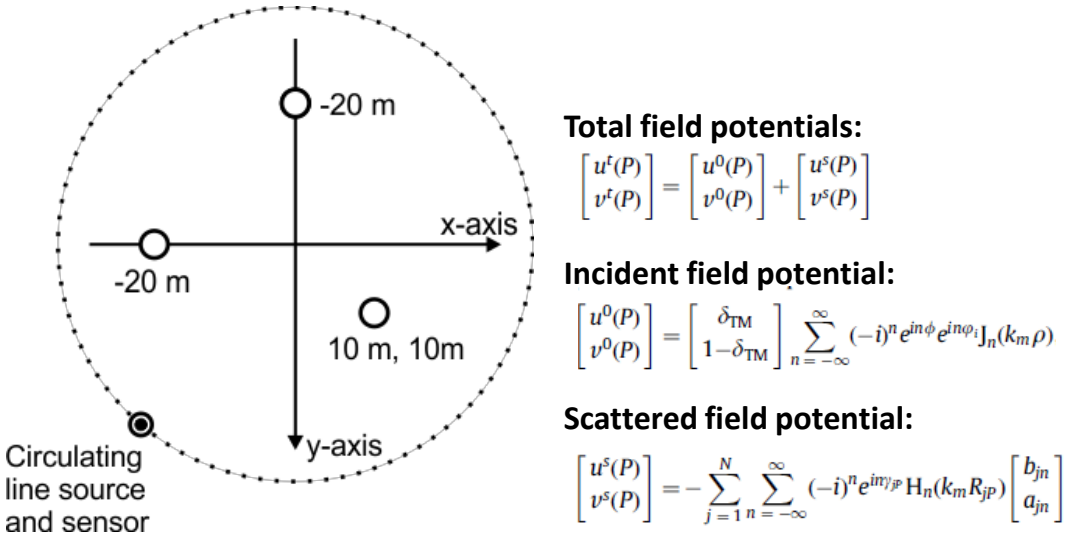

Figure 18. ***Total, incident, and scattered field potentials from circulating line source.***

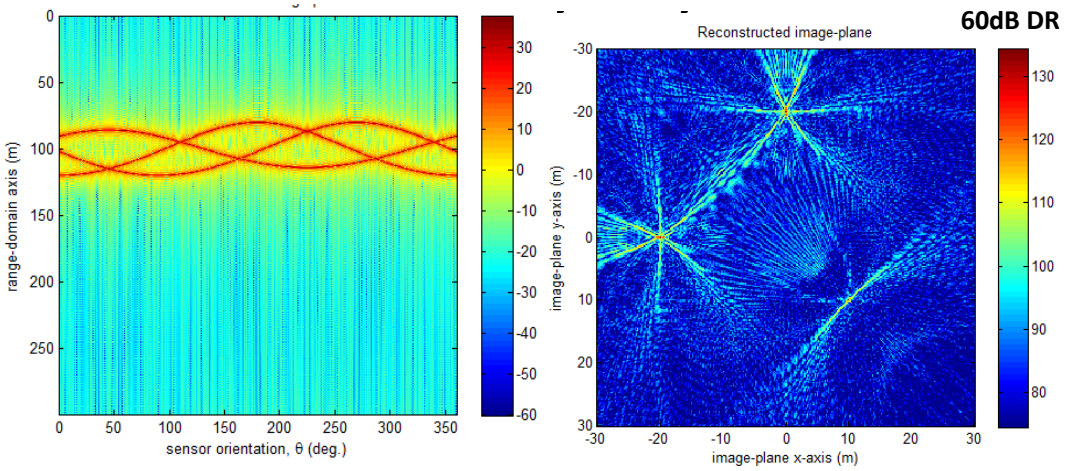

Figure 19. ***Example of reconstructed image from the three sensors.***

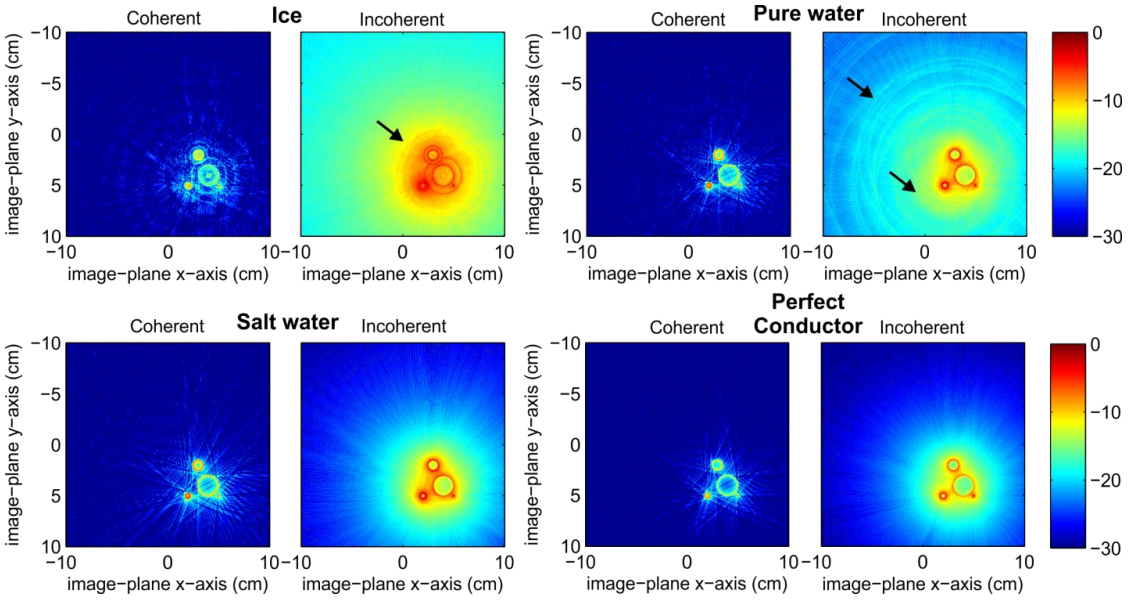

Figure 20. ***As an example, these plots show a small collection of four targets being imaged using coherent and incoherent versions of the time-domain back-projection inversion. The particles are of different sizes and the image-plane is shown for particles that have properties of ice, pure water, salt water, and the ideal target case of perfect conductors. Even in this simple example, we see the artifacts of scattering in the image due to low-loss dielectrics. Coherent imaging is shown to reduce these artifacts considerably when compared to incoherent imaging.***

VIII. Numerical Results and Discussion

The simulation results shown in Figure 21 were obtained by commanding the grains to conform to a prescribed optical surface. The cloud is first shaped into a disk, then into a paraboloid of specified focal length and diameter.

The numerical results indicate that the force required to shape 1 meter diameter disk into parabola is of the order of 10^{-8} N. Assuming a grain shape which is asymmetric to incoming light, the torque required to align 1 micron grain is of the order of 10^{-15} Nm. Figure 22 shows the results of the integrated simulation of coherent and incoherent imaging of a growing cloud. Figure 23 shows the results of the integrated simulation of coherent and incoherent imaging of a variable geometry cloud. Figure 24 and 25 show the components of the Electric and Magnetic field, as a function of Julian date, involved in the trapping mechanism required to rigidly retarget the parabolic shaped cloud of 60 degrees about the x-axis (in cloud body frame).

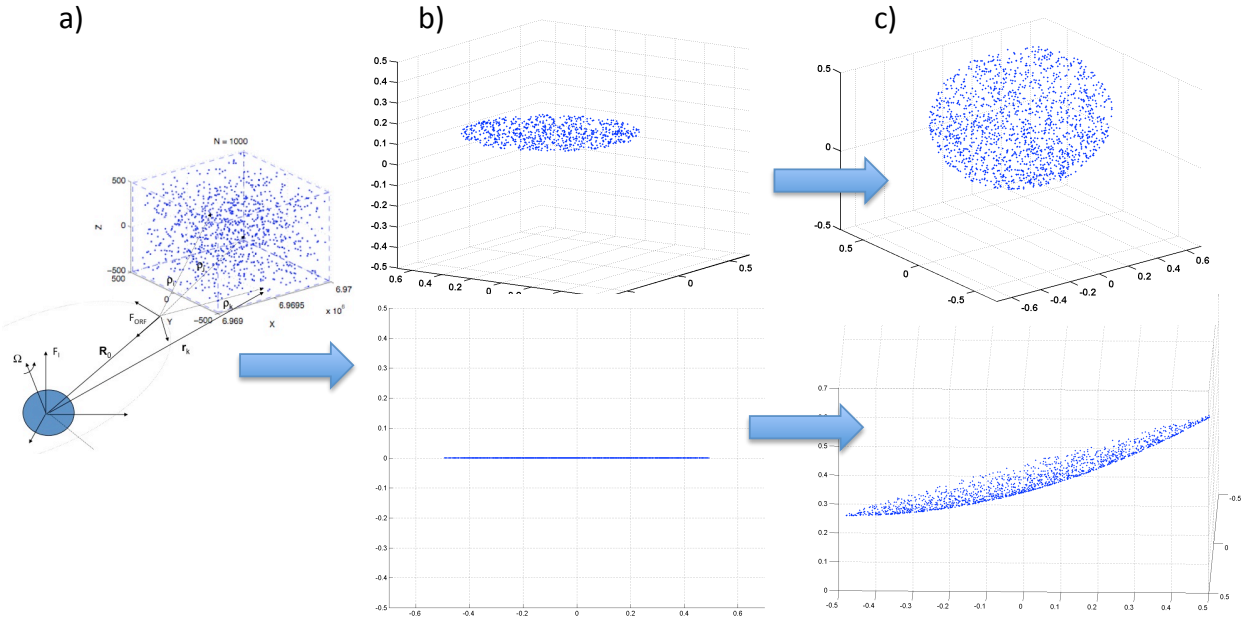

Figure 21. **Re-shaping of a) amorphous cloud to b) disk and c) paraboloid.**

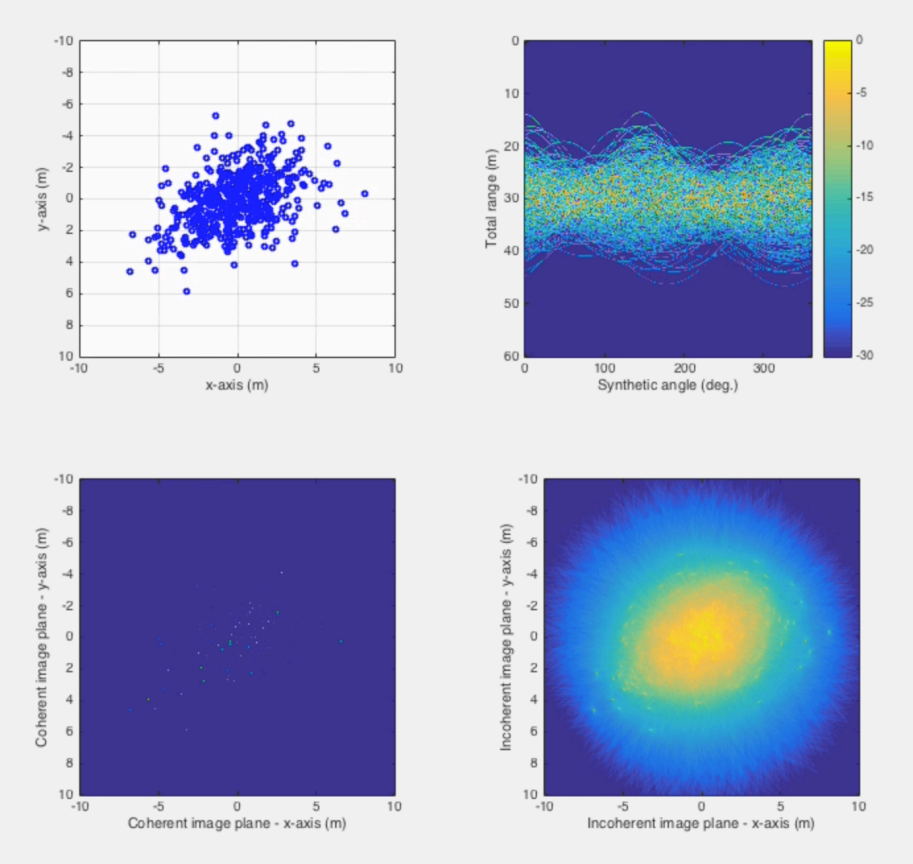

Figure 22. **Simulation of coherent and incoherent imaging of a growing cloud.**

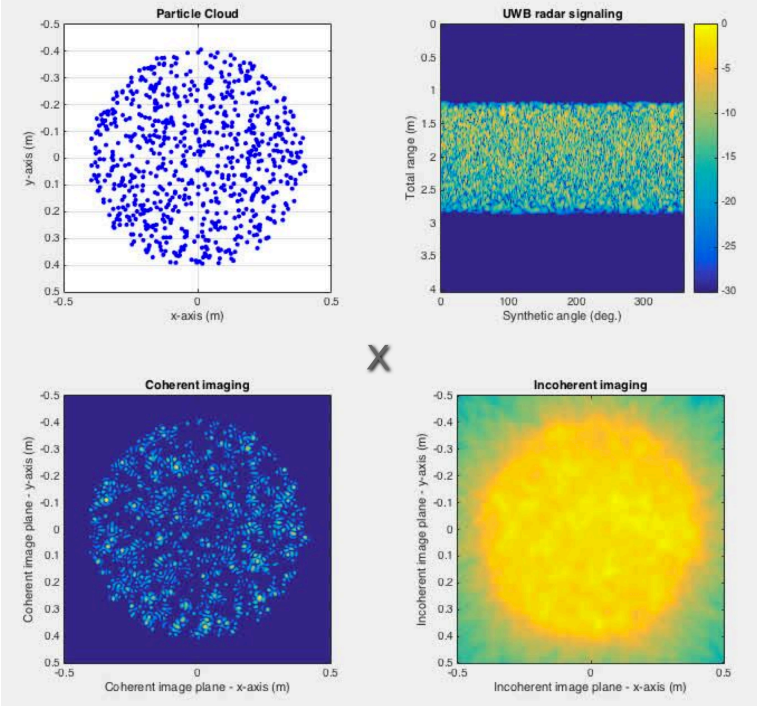

Figure 23. **Simulation of coherent and incoherent imaging of a variable geometry cloud.**

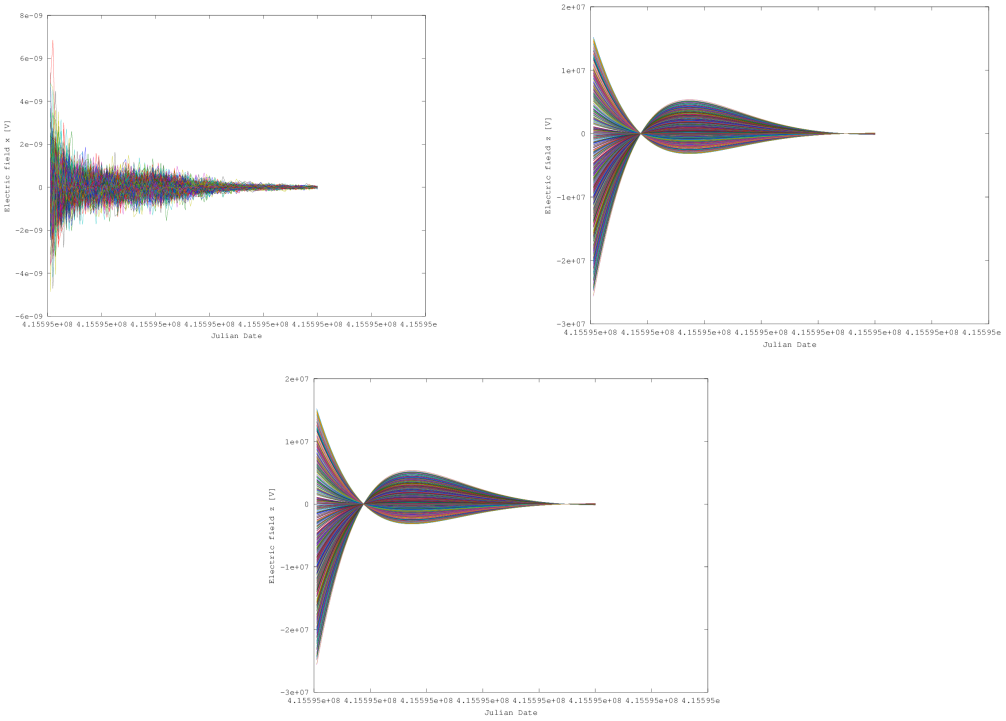

Figure 24. **Components of Electric field, as a function of Julian date, involved in the trapping mechanism required to rigidly retarget the parabolic shaped cloud of 60 degrees about the x-axis (in cloud body frame).**

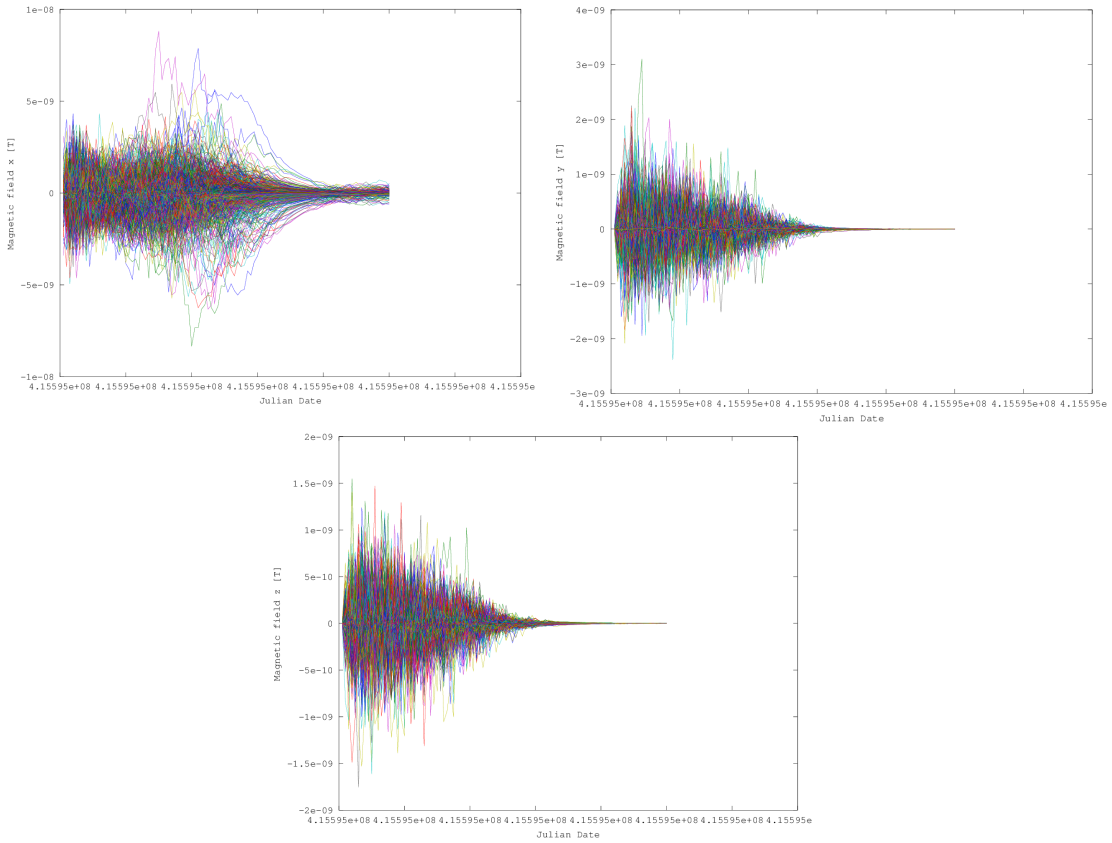

Figure 25. **Components of Magnetic field, as a function of Julian date, involved in the trapping mechanism required to rigidly retarget the parabolic shaped cloud of 60 degrees about the x-axis (in cloud body frame).**

IX. Conclusion

In this paper, we have presented some ideas regarding the modeling, dynamics and control aspects of *granular spacecraft*. We have addressed the modeling and autonomous operation of a distributed assembly (the cloud) of large numbers of grains, controlled by opto-mechanical interactions. The modeling and simulation of a representative concept was also discussed. The application considered so far was a reflective imaging system for astrophysics, but many unexplored applications of granular spacecraft are yet to be discovered.

Acknowledgments

This research was carried out at the Jet Propulsion Laboratory, California Institute of Technology, under a contract with the National Aeronautic and Space Administration. The authors are grateful to Prof. Grover Swartzlander of Rochester Intitute of Technology and his students Ms. Xiaopeng Peng, and Ms. Alexandra Artusio-Glimpse for the work done in blind image deconvolution and optical ray tracing, described elsewhere.

References

[1] Ashkin, A.: Acceleration and trapping of particles by radiation pressure, Phys. Rev. Lett. **24**. 156-159, 1970.

[2] Axelrad, D.R.: Micromechanics of Solids, Elsevier Scientific Publishing Company, Amsterdam, 1978.

[3] Born, M., and Wolf, E.: *Principles of Optics*, 2nd edition, Pergamon Press, 1964, pp. 400.

[4] Brady, D.J., Hagen, N.: *Multiscale lens design*, Opt. Express 17, 10659-10674, 2009.

[5] Eringen ,C.: Microcontinuum Field Theories, Springer Verlag, 1999.

[6] Fuchs, N.A.: *The Mechanics of Aerosols*, Dover Publications, 1989.

[7] Gazi, V., and Passino, K.: Stability Analysis of Clouds, Proc. Of the American Control Conference, Anchorage, AK, May 8-10, 2002, pp. 1813-1818.

[8] Ghanem, R., and Spanos, P.: Stochastic Finite Elements, a Spectral Approach, Dover Publications, New York, 2003.

[9] Greengard, L.: The numerical solution of the N-body Problem, Computers in Physics, March-April 1990, pp. 142-152.

[10] Grzegorczyk, T., Kemp, B. A., Kong, J.A.: Trapping and binding of an arbitrary number of cylindrical particles in an in-plane electromagnetic field, J. Opt. Soc. Am. A, 23(9) Sept. 2006.

[11] Grzegorczyk, T., Kemp, B. A., Kong, J.A.: *Passive guiding and sorting of small particles with optical binding forces*, Opt. Lett., 31(22), Nov. 2006.

[12] Kadowaki, H., and Liu, W.K.: A Multiscale Approach for the Micropolar Continuum Model, Computer Modeling in Engineering and Science, 2005, vol.7, no. 3, pp. 269-282.

[13] Kokhanovsky. A. A.: *Cloud Optics*, Springer, 2006.

[14] Labeyrie, A.: Standing Wave and Pellicle: A Possible Approach to Very Large Space Telescopes, Astronomy and Atrophysics, 77, L1-L2, 1979.

[15] Lerman, K., Martinoli, A., Galstyan, A.: *A Review of Probabilistic Macroscopic Models for Swarm Robotic Systems*, in Swarm Robotics Workshop: State-of-the-art survey, edited by E. Sahin and W. Spears, LCNS 3342, Springer-Verlag, Berlin, 2005, pp.143-152.

[16] Mettler E., Breckenridge W.G., and Quadrelli M.B.: *Large Aperture Telescopes in Formation: Modeling, Metrology, and Control,* The Journal of the Astronautical Sciences, vol. 53, no.5 October-December 2005, pp.391-412.

[17] Mogilner, A., Edelstein-Keshet, L.: A Non-local Model for a Cloud, Journal of Mathematical Biology, 1999, no. 38, pp. 534-570.

[18] Molmud, P., "Expansion of a Rarefield Gas Cloud into a Vacuum," The Physics of fluids 3, 362-366 (1960).

[19] Palmer, A.J.: *Radiation-induced Orientation of Atmospheric Aerosols*, J. OP. Soc. America A, vol. 8, no. 2, February 1991.

[20] Pfalzner, S, and Gibbon, P.: Many-Body Tree Methods in Physics, Cambridge University Press, 1996.

[21] Quadrelli, M., Basinger, S., Swartzlander, G.: *Dynamics and Control of a Disordered System In Space*, AIAA SPACE 2013 Conference, San Diego, Ca, Sept. 2013.

[22] Reif, J.H., and Wang, H., Social Potential Fields: A Distributed Behavioral Control for Autonomous Robots, Robotics and Autonomous Systems 27 (1999) 171-194.

[23] Siljak, D.D.: Decentralized Control of Complex Systems, Academic Press, 1990.

[24] Schuster, D.L: Dynamic Response of Dielectric Lenses Influenced By Radiation Pressure, M.S. Thesis , R.I.T., 2014.

[25]Stephen H. Simpson, Simon Hanna, Timothy J. Peterson, and Grover A. Swartzlander, "Optical lift from dielectric semicylinders," Opt. Lett. 37, 4038-4040 (2012).

[26] Van de Hulst, H. C.: *Light Scattering by Small Particles*, Dover Publications, 1981.

[27]Quadrelli, M., et al.: *Dynamics and Control of a Disordered System In Space,* AIAA SPACE 2013 Conference, San Diego, Ca, Sept. 2013. Also, NIAC Phase I final report on Orbiting Rainbows task, 2013.